Pressure-induced amorphization of $YVO_4:Eu^{3+}$ nanoboxes

2016 Nanotechnology 27 025701

(http://iopscience.iop.org/0957-4484/27/2/025701)

IOP Publishing Nanotechnology
Nanotechnology 27 (2016) 025701 (8pp) doi:10.1088/0957-4484/27/2/025701

Pressure-induced amorphization of YVO_4: Eu^{3+} nanoboxes

J Ruiz-Fuertes[1], O Gomis[2], S F León-Luis[3], N Schrodt[1,10], F J Manjón[4], S Ray[4,5], D Santamaría-Pérez[6], J A Sans[4], H M Ortiz[4,7], D Errandonea[6], C Ferrer-Roca[6], A Segura[6], D Martínez-García[6], V Lavín[8], U R Rodríguez-Mendoza[8] and A Muñoz[9]

[1] Institut für Geowissenschaften, Goethe-Universität, Altenhöferallee 1, D-60438 Frankfurt am Main, Germany
[2] Centro de Tecnologías Físicas, Universitat Politècnica de València, E-46022 Valencia, Spain
[3] Departamento de Física, Universidad de La Laguna, E-38200 San Cristóbal de La Laguna, Santa Cruz de Tenerife, Spain
[4] Instituto de Diseño para la Fabricación y Producción Automatizada, Universitat Politècnica de València, E-46022 Valencia, Spain
[5] Department of Chemistry, AISECT University, Bhopal, India
[6] Departamento de Física Aplicada-ICMUV, Universitat de València, E-46100 Burjassot, Valencia, Spain
[7] CINVESTAV-Departamento de Nanociencia y Nanotecnología, Universidad Quertaro, Quertaro, Mexico
[8] Departamento de Física Fundamental y Experimental, Electrónica y Sistemas, Universidad de La Laguna, E-38200 San Cristóbal de La Laguna, Santa Cruz de Tenerife, Spain
[9] Departamento de Física, Instituto de Materiales y Nanotecnología, Universidad de La Laguna, E-38205 La Laguna, Tenerife, Spain

E-mail: ruiz-fuertes@kristall.uni-frankfurt.de

Received 27 July 2015, revised 7 October 2015
Accepted for publication 14 October 2015
Published 30 November 2015

Abstract

A structural transformation from the zircon-type structure to an amorphous phase has been found in YVO_4:Eu^{3+} nanoboxes at high pressures above 12.7 GPa by means of x-ray diffraction measurements. However, the pair distribution function of the high-pressure phase shows that the local structure of the amorphous phase is similar to the scheelite-type YVO_4. These results are confirmed both by Raman spectroscopy and Eu^{3+} photoluminescence which detect the phase transition to a scheelite-type structure at 10.1 and 9.1 GPa, respectively. The irreversibility of the phase transition is observed with the three techniques after a maximum pressure in the upstroke of around 20 GPa. The existence of two $^5D_0 \rightarrow {}^7F_0$ photoluminescence peaks confirms the existence of two local environments for Eu^{3+}, at least for the low-pressure phase. One environment is the expected for substituting Y^{3+} and the other is likely a disordered environment possibly found at the surface of the nanoboxes.

Keywords: high pressure, amorphization, nanocrystal

(Some figures may appear in colour only in the online journal)

1. Introduction

The structural behavior of nanomaterials under compression usually varies from the bulk due to the important role of the surface in the structure stabilization [1]. In fact, several works performed on zircon-type (space group $I4_1/amd$) compounds have shown that, in general, the high-pressure behavior of the nanomaterial cannot be extrapolated from the behavior of the bulk. For instance, bulk zircon-type YPO_4 transforms to a scheelite-type structure (space group $I4_1/a$) passing through a monazite-type structure (space group $P2_1/n$) while nanocrystals of this compound directly transform from zircon to scheelite [2–4]. In $YCrO_4$ the opposite occurs [5]. In addition, an interesting effect can be found in the propensity of

[10] Née N Rademacher.

nanomaterials to undergo the so called pressure-induced amorphization (PIA) [4, 6]. The density of surface defects can increase abruptly in the surrounding of a phase transition eventually giving rise to its frustration [1]. Far from being a problem, interesting physical properties can arise upon amorphization [7, 8], especially if the amorphization is irreversible.

YVO_4 crystallizes in a zircon-type structure where the V and Y cations are four-fold and eight-fold coordinated, respectively. YVO_4, doped with Eu^{3+} or other rare Earth ions has been extensively studied for more than three decades and it is currently employed as a bright red-emitting phosphor in optical devices as cathode ray tubes and fluorescent lamps [9, 10]. It has been proposed as a refractive index sensor [11], and also as a red nanophosphor in nanosize probes for drug delivery systems [4, 12, 13]. Under high pressure bulk YVO_4 undergoes a structural phase transition to a scheelite-type structure at 7.5 GPa [14–16] as most zircon compounds. However, what happens to their nanocrystals is still unknown.

In this work, we report on the irreversible PIA above 12.7 GPa in the technologically important europium-doped yttrium vanadate (YVO_4:Eu^{3+}) nanoboxes with lateral size of 20 nm. We have studied the high-pressure structural phase transition of YVO_4:Eu^{3+} nanoboxes from both long-range and local approaches by means of x-ray diffraction (XRD), including pair distribution function (PDF) analysis, Raman spectroscopy, and Eu^{3+} photoluminescence.

2. Experimental details

YVO_4:Eu^{3+} nanoboxes with 20 nm lateral size were synthesized using a surfactant-assisted route with an annealing temperature of 800 °C [17]. In the YVO_4:Eu^{3+} nanoboxes the concentration of Eu^{3+} was 4 at.wt% with respect to Y^{3+}. Ambient pressure characterization of the samples was performed by a $K_{\alpha1}$:$K_{\alpha2}$ Cu radiation in a conventional Rigaku Ultima IV diffractometer and by transmission electron microscopy (TEM). Samples for TEM were deposited onto 300 mesh copper TEM grids coated with 50 nm carbon films. Nanocrystals dispersed in acetone were placed on the grid dropwise. The excess liquid was allowed to evaporate in air. A Tecnai G2 F20 field emission gun under an acceleration voltage of 200 kV was used for TEM measurements. High-pressure experiments were performed using either a membrane-type diamond anvil cell (DAC) with 500 μm culets and a 45 μm stainless steel gasket with a 250 μm hole or a large-opening Boehler-Almax DAC [18] with 350 μm culets and a 40 μm tungsten gasket with a 150 μm hole. In all experiments we loaded in the DAC powder pellets together with some ruby chips as pressure markers [19] and a mixture of methanol-ethanol-water (16:3:1) was employed as pressure transmitting medium. We performed three high-pressure powder XRD experiments. Two of them were carried out using the membrane-type DAC at I15 beamline in Diamond Light Source (run1 and run2) and a third one was carried out at the EC beamline P2.02 at PETRA III (run3) with a Boehler-Almax DAC. In the experiments performed at Diamond we reached a maximum pressure of 17.2 GPa with $\lambda = 0.4132$ Å (run1) and 21.5 GPa with $\lambda = 0.4246$ Å (run2). In both experiments the x-ray beam was focused down to 40 × 40 μm^2 using Kirkpatrick–Baez (KB) mirrors. The images were collected using a MAR345 image plate located at 425 and 350 mm from the sample for run1 and run2, respectively. The objective of the experiment performed at PETRA III (run3) was to obtain a high Q-range diffractogram of the amorphous phase of the YVO_4 nanoboxes at 21 GPa to determine the PDF. For this purpose, we used an x-ray wavelength of $\lambda = 0.29067$ Å and a beam focused down to 2.1 × 2.4 μm^2 to measure independently the scattering of the sample and the background for an accurate background correction. A Perkin Elmer detector was used and placed at 320 mm from the sample. The diffraction patterns were integrated as a function of 2θ using FIT2D in order to give conventional, one-dimensional diffraction profiles [20]. The indexing and refinement of the powder diffraction patterns was performed using the Unitcell [21], POWDERCELL [22], and GSAS [23, 24] program packages. The PDF was obtained by a Fourier transform of the corrected and normalized diffraction pattern using standard procedures and those unique to area detectors implemented in the program PDFgetX [25] which are described in Chupas *et al* [26]. The diffractogram was terminated at a Q_{max} of 9 $Å^{-1}$. PDF simulations were perfomed with the program PDFgui [27]. The Raman spectroscopy and photoluminescence experiments were carried out using the membrane-type DAC in backscattering geometry with the $\lambda = 532$ nm line of a Nd:YAG laser employing a confocal LabRam HR UV microRaman single spectrometer with resolution better than 2 cm^{-1} (0.04 nm).

3. Results and discussion

3.1. Sample characterization

The Rietveld refinement of the XRD pattern of nanoboxes of YVO_4:Eu^{3+} taken at ambient conditions is shown in figure 1. All reflections can be indexed to the zircon-type structure of YVO_4 with lattice parameters and unit-cell volume of $a = 7.125(1)$ Å, $c = 6.296(1)$ Å, and $V_0 = 319.6(1)$ $Å^3$. Nanoboxes exhibit a V_0 around 0.14 % larger than that previously reported for the bulk [15] ($V_0 = 319.15(1)$ $Å^3$). Similar results have been observed in nanoparticles of other compounds [28].

In order to determine the size of the YVO_4:Eu^{3+} nanoboxes, we have used the full width at half maximum of the (200) Bragg reflection (figure 1) and the Scherrer formula with a Scherrer constant of 0.89 for the case of cubic crystallites [29]. Our estimation has taken into account the correction for the x-ray instrumental broadening. The result gives a mean size value for the nanoboxes of 18(2) nm. In figure 2 we show a TEM micrograph and a HRTEM micrograph focused on a group of nanoparticles of YVO_4:Eu^{3+} and on a single particle, respectively. It can be seen that the size observed for a single nanoparticle is around 20 nm supporting the estimation made by XRD. In addition, the

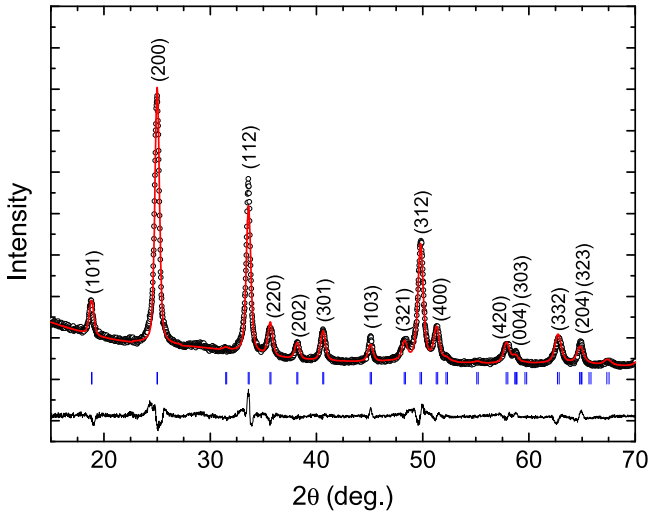

Figure 1. X-ray diffraction pattern of YVO_4:Eu^{3+} nanoboxes at ambient conditions with the Rietveld refinement. Experimental data are plotted as empty circles and the calculated difractogram and the residual as solid lines. The numerical values for the residuals are $R_p = 2.4\%$ and $R_{wp} = 3.2\%$. Bragg reflections are indicated with vertical ticks.

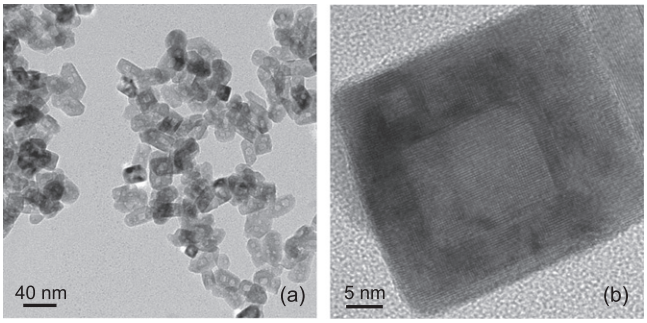

Figure 2. (a) TEM micrograph of a group of YVO_4:Eu^{3+} nanoboxes and (b) HRTEM micrograph of a single nanoparticle.

HRTEM image of the single nanobox shows the perfect alignment of the crystallographic planes of the top surface of the nanoparticle, thus indicating that the nanoboxes are single crystals.

3.2. X-ray diffraction

A selection of XRD patterns at different pressures and three shots of the image-plate from run2 are shown in figure 3. Along the experiment the integration time was kept constant, what let us compare the background changes as pressure is increased. As observed from the three image plate photographs, the rings from the low-pressure phase of YVO_4 are sharp at 0.6 GPa, very broad at 12.7 GPa, and only two halos are observed at 21.5 GPa. Up to 12.7 GPa, reflections shift to higher 2θ angles as a result of the lattice compression. Around 12.7 GPa, the background increases, probably due to the solidification of the presure transmiting medium leading to the loss of hydrostatic conditions [30] (∼10 GPa). At higher pressures, the intensity of the reflections decreases and a distribution of broad features emerged pointing out the

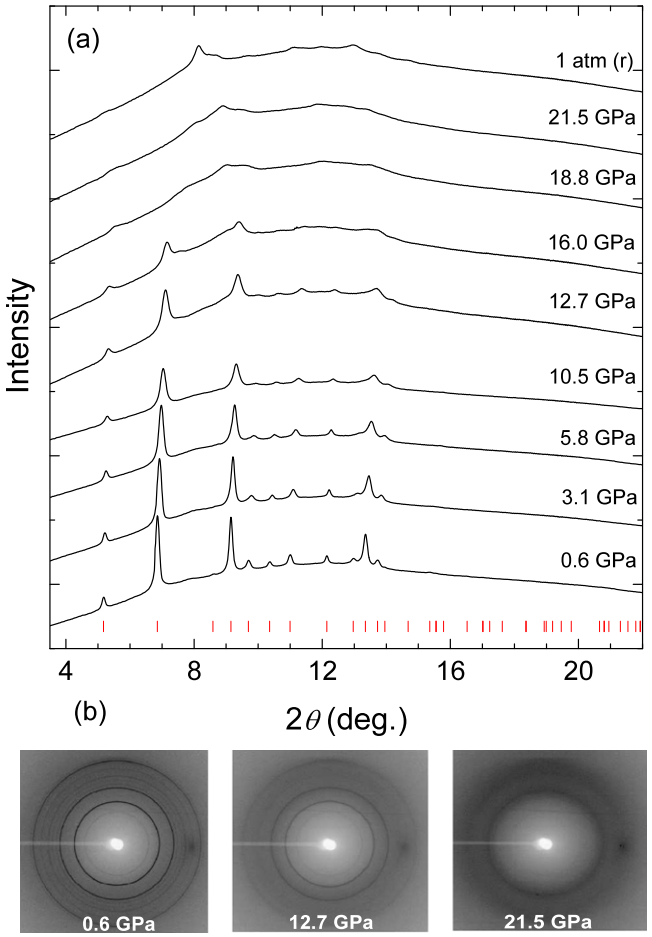

Figure 3. (a) Selection of x-ray diffractograms of YVO_4:Eu^{3+} nanoboxes at different pressures from run2. Vertical ticks at 0.6 GPa indicate the Bragg reflections. (b) Image plate shots at three different pressures showing the evolution of the x-ray diffraction rings along the amorphization of YVO_4:Eu^{3+}.

amorphization of our sample. At 18.8 GPa, the absence of reflections from the low-pressure phase indicates that the amorphization of our sample has concluded. The diffractogram obtained after releasing pressure included at the top of figure 3 shows that the amophization process is irreversible. The amorphous features appear slightly sharper as a consequence of the released stress.

The observed amorphization of the YVO_4 nanoboxes above 12.7 GPa contrasts with the structural phase transition observed in the bulk from the zircon to the scheelite-type structure at 7.5 GPa [15, 16]. However, as we have shown in figure 3, the amorphous phase of nano YVO_4 shows a distinctive bump located at 8.5° at 18.8 GPa, where no reflections from the low-pressure zircon phase of YVO_4 are expected. The presence of bumps in the x-ray diffractograms is usually indicative of short-range order in the amorphous, which in the case of nano YVO_4 must be different from the low-pressure phase. Unfortunately, no structural determination can be done from the diffractograms measured above 16 GPa since there is no long-range order. In order to investigate the short-range order of the amorphous phase of the YVO_4 nanoboxes we performed an experiment (run3) to

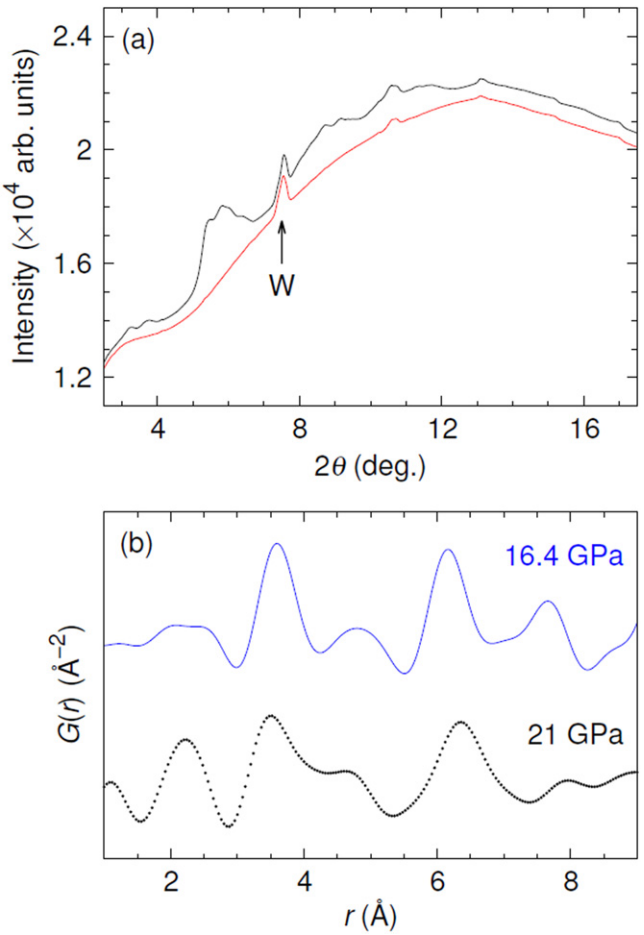

Figure 4. (a) Diffractograms of YVO_4:Eu^{3+} nanoboxes (black solid line) and the background (red dashed line) measured at 21 GPa. The W marks the position of a reflection from the tungsten gasket that was unavoidable due to the divergence of the beam. (b) Calculated PDF for the scheelite-type structure of bulk YVO_4 at 16.4 GPa [15] (solid blue line) and experimental PDF for the amorphous phase of the YVO_4:Eu^{3+} nanoboxes at 21 GPa after the background correction (black dotted line).

determine the PDF of the amorphous phase at 21 GPa. The resolution of the PDF is related to the Q-range measured. For this reason, we employed a short wavelength ($\lambda = 0.29067$ Å) monochromatic x-ray beam and a large opening ($4\theta \sim 90°$) DAC as previously commented. The diffractogram of the sample at 21 GPa as well as the background at the same conditions are shown in figure 4(a).

An important step in the determination of the PDF of an amorphous phase is the correct removal of the background. For this reason, we measured at the same pressure both the diffractogram of the sample and the background. Once the background is removed, the final diffractogram is Fourier transformed to real space obtaining the distribution of the interatomic distances plotted in figure 4(b) where the generated PDF is compared with the calculated one from the scheelite structure of bulk YVO_4 obtained at 16.4 GPa by Wang *et al* [15]. As can be seen in figure 4(a), the diffractogram contained reflections from the tungsten gasket which caused a slight inaccuracy in the background

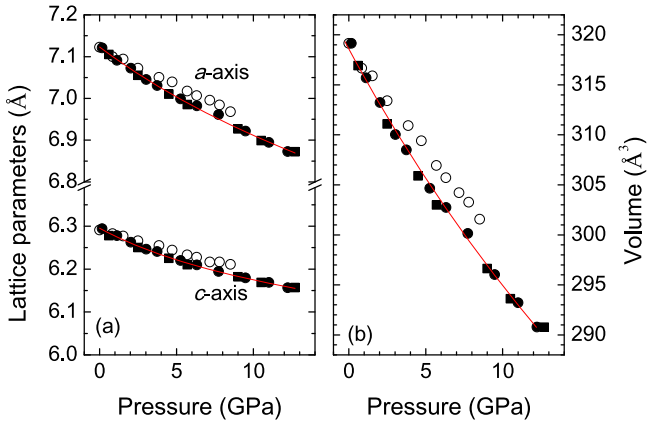

Figure 5. (a) Pressure dependence of the lattice parameters a and c and (b) unit-cell volume V of YVO_4. Filled circles and squares correspond to data of nano YVO_4:Eu^{3+} obtained in run1 and run2, respectively. Empty circles correspond to data for bulk YVO_4 reported by Wang *et al* [15]. Continuous lines are the Murnaghan and second-order Birch–Murnaghan equations of state fits to the lattice parameters and volume, respectively.

determination and the resulting PDF. The apparent difference in the PDFs at around 2 Å can be explained by correlated atomic motion. It is well known that experimental PDFs have sharper peaks at low r values than the corresponding simulated PDFs because of correlated motion of neighboring atoms [31]. The positions of the peaks in the experimental PDF are shifted to smaller r values up to a distance of around 5 Å and to larger r values at $r > 5$ Å. The shift to smaller r values can be explained by the larger pressure of 21 GPa compared to 16.4 GPa. The shift to larger r values shows that the amorphous phase is not as ordered as the crystal would be. However, the overall shape of the PDF curves is very similar indicating that the local structure of the YVO4:Eu^{3+} nanoboxes is of scheelite-type.

In figure 5 we show the pressure dependence of the lattice parameters and the unit-cell volume V for zircon-type nano YVO_4 from our XRD experiments and for bulk YVO_4 taken from the literature [15]. The experimental axial compressibilities for a and c axes at ambient pressure, defined as $\kappa_x = -(1/x)(\partial x/\partial P)$ and obtained by the fitting of a Murnaghan equation of state (EOS) [32], are $\kappa_a = 3.9(2) \times 10^{-3}$ GPa^{-1} and $\kappa_c = 3.1(2) \times 10^{-3}$ GPa^{-1}. Our experiments show an anisotropy in the axial compression being the a-axis more compressible than the c-axis. We have also estimated the axial compressibilities for the case of bulk YVO_4 from Wang *et al* [15] data, measured with N_2 as pressure transmitting medium. Those data yield values of $\kappa_a = 2.5(2) \times 10^{-3}$ GPa^{-1} and $\kappa_c = 1.7(2) \times 10^{-3}$ GPa^{-1} which also shows the anisotropy in the axial compression for the bulk case. In order to compare the compressibility of the bulk and the nanocompound we fitted both bulk [15] and nano data to a second-order Birch–Murnaghan [33] EOS. We obtained for nano YVO_4 a bulk modulus $B_0 = 111(2)$ GPa, which is approximately 23% smaller than that obtained for bulk YVO_4 ($B_0 = 136(2)$ GPa). This indicates that nano YVO_4 is more compressible than bulk YVO_4. In our case the decrease of

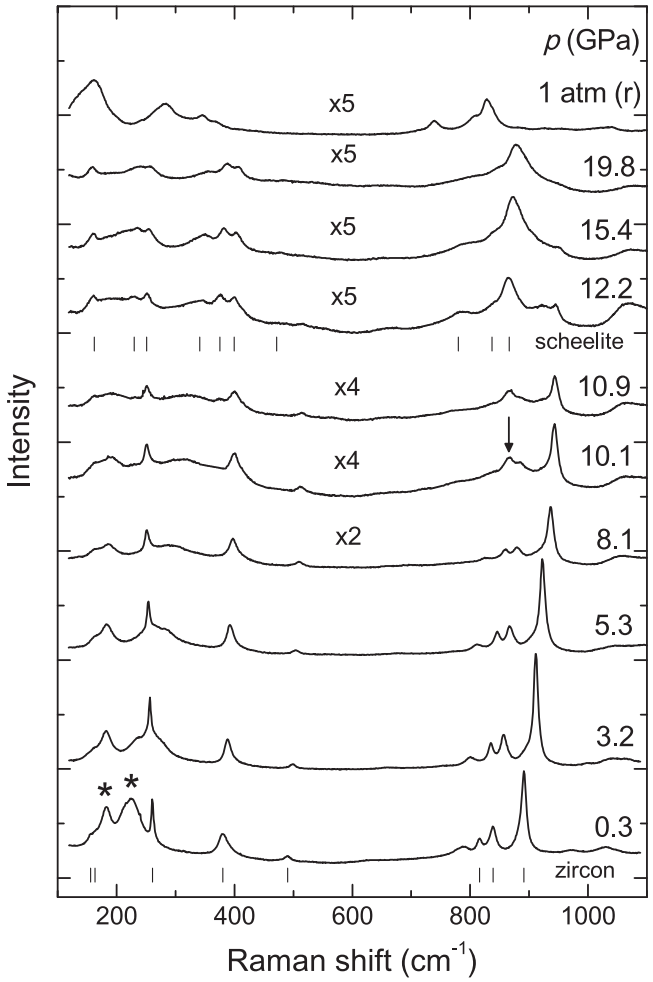

Figure 6. Raman spectra of YVO_4:Eu^{3+} nanoboxes at different pressures. Vertical ticks show the experimental frequencies of the observed first-order Raman modes for the zircon and scheelite phases. Asterisks mark the tentatively assigned second-order modes. The vertical arrow at 10.1 GPa indicates the appearance of a Raman band attributed to the high-pressure phase. The zoom applied in each spectrum is shown.

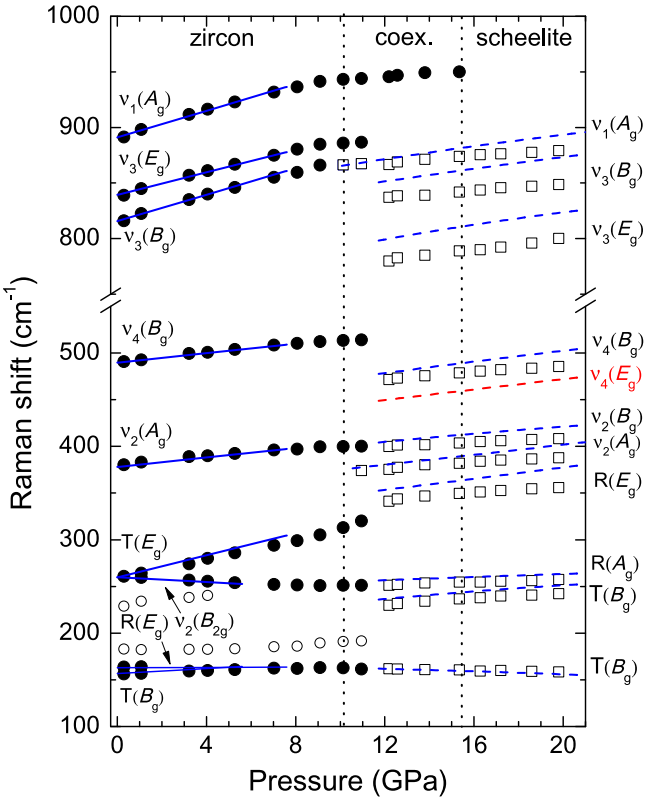

Figure 7. Pressure dependence of the experimentally observed first-order (solid circles) and second order (empty circles) Raman active modes of the low-pressure and high-pressure (empty squares) phases of YVO_4:Eu^{3+} nanoboxes. For comparison, the fits for bulk YVO_4 (solid and dashed blue lines) are also given [16]. The red dashed line shows the $\nu_4(E_g)$ mode not detected in our experiment with YVO_4:Eu^{3+} nanoboxes, but present in the bulk. The vertical black dashed lines represent the onset and end of the phase transition. ν_i stands for the internal modes of the VO_4 molecule and R and T represent the pure rotation and translation of the VO_4 molecule [16].

particle size produces an increase in compressibility in contrast with results reported in other compounds, suggesting an inverse Hall–Petch behavior in nanocrystalline YVO_4 as observed recently in nanocrystalline-TiO_2 [34].

3.3. Raman spectroscopy

In order to support the evidence found with XRD of a PIA with a short-range scheelite-type order, we have employed Raman spectroscopy, which is known to be a much more local technique, sensitive to investigate materials with short-range order.

In figure 6 we show a selection of Raman spectra of YVO_4:Eu^{3+} nanoboxes at different pressures up to 19.8 GPa. At low pressure, we can see 9 out of 12 first-order Raman active modes of zircon-type YVO_4 in good agreement with previous Raman spectroscopy measurements on the bulk [14, 16]. Additionally, we also see two extra broad bands highlighted by asterisks which shift fast with pressure and whose origin is tentatively assigned to second-order Raman modes. The Raman spectra up to 9.1 GPa can be attributed to the zircon phase. At 10.1 GPa, the intensity drops down and an extra band at around 866.2 cm^{-1} emerges (figure 6) indicating the onset of the phase transition in good agreement with XRD. At higher pressures, the intensity of the modes corresponding to the low-pressure phase keeps decreasing while extra bands corresponding to the high-pressure phase emerge. Above 15.4 GPa, the phase transition is complete with the Raman spectrum resembling that of the scheelite phase of bulk YVO_4 [16]. As pressure is increased to 19.8 GPa, 10 first-order Raman active modes of the scheelite phase are observed to shift with pressure. Finally, the irreversibility of the phase transition in our nanocrystals is also observed by Raman spectroscopy as shown by the Raman spectrum of the recovered sample shown at the top of figure 6 when compared to the Raman spectrum of recovered samples from 33 GPa in bulk YVO_4 [16].

In correlation with the XRD results presented before (section 3.2), the observed intensity decrease of the Raman spectra and the progressive band broadening above 10.9 GPa correlates well with the amorphization observed by XRD

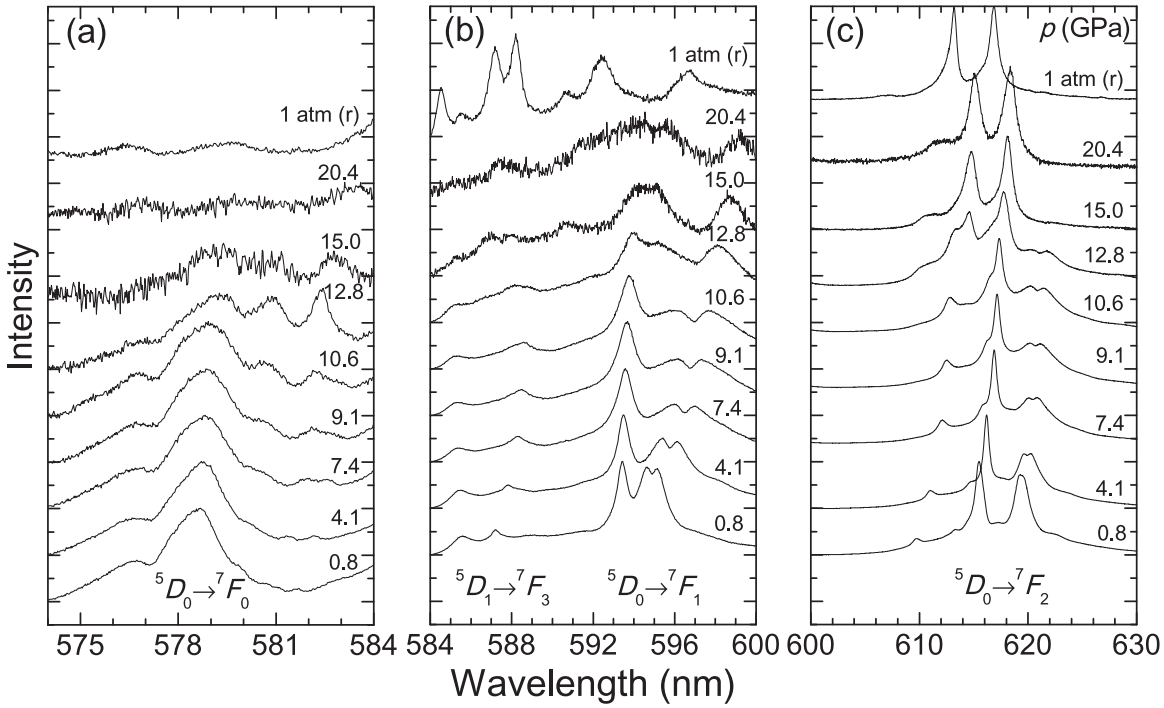

Figure 8. Eu^{3+} photoluminescence spectra at different pressures up to 20.4 GPa showing the (a) $^5D_0 \rightarrow {}^7F_0$, (b) $^5D_1 \rightarrow {}^7F_3$ and $^5D_0 \rightarrow {}^7F_1$, and (c) $^5D_0 \rightarrow {}^7F_2$ normalized emission bands with respect to the most intense peak of the range.

above 12.7 GPa. On the other hand, the emergence of an additional band at 10.1 GPa correlates well with the onset of the phase transition to a scheelite-type structure in the short-range order. This evidence is supported by the comparison of the pressure dependence of the Raman mode frequencies of YVO_4:Eu^{3+} nanoboxes and bulk YVO_4 shown in figure 7.

For the low-pressure zircon phase the agreement up to 7.5 GPa (when the bulk undergoes a phase transition) is excellent. The main difference between bulk and nano YVO_4 is observed in the behavior change of the highest frequency $\nu_1(A_g)$ mode. In nanoboxes, this mode decreases its pressure coefficient during the coexistence range from 10.1 to 15.4 GPa, probably as an effect of the surrounding coexisting scheelite phase. Regarding the high-pressure scheelite phase the agreement is also good although the frequencies of the nano YVO_4 are shifted to lower values with respect to the bulk and the weak $\nu_4(E_g)$ mode is not detected in the nanoboxes.

3.4. Photoluminescence

An interesting question still to solve is the effect of the PIA and short range phase transition to a scheelite-type structure on the local structure of Eu^{3+} ions. For this reason we have studied the photoluminescence of YVO_4:Eu^{3+} nanoboxes under pressure. Eu^{3+} ion is ideal not only to confer photoluminescence to the nano YVO_4 for technological applications [4, 9, 10, 12, 13], but also to obtain local information of changes at the local crystalline structure by the analysis of its emission spectrum [35, 36]. This is due to its electronic energy levels scheme which consists of seven ^7F_J ($J = 0$–6) multiplets spaced almost uniformly and five ^5D_J ($J = 0$–4) multiplets well separated in energy [37]. In this energy structure, the levels with the lowest energies, $^7F_0$ and $^5D_0$, are non-degenerated. This implies that the crystal field interaction between the electrons of the oxygen ligands and the 4f electrons of the Eu^{3+} ions, responsible of its optical properties, cannot split these levels and, hence, the $^5D_0 \rightarrow {}^7F_0$ transition gives rise to a single peak [38]. Therefore, any additional peak observed and associated with this transition in the Eu^{3+} emission spectra would be directly related with the presence of more than one available site for Eu^{3+}.

A selection of photoluminescence spectra of YVO_4:Eu^{3+} nanoboxes are shown in figure 8 where the spectra have been split in three graphs and normalized in different relative scales to facilitate comparison of photoluminescence spectra at different pressures. The $^5D_0 \rightarrow {}^7F_1$ transition from 593 to 598 nm (figure 8(b)) is magnetic dipole in nature and therefore, the existence of three overlapped peaks for this transition is the first indication that Eu^{3+} ions occupy a low-symmetry environment even at low pressure. In contrast, the $^5D_0 \rightarrow {}^7F_0$ transition from 576 to 579 nm (figure 8(a)) and the $^5D_0 \rightarrow {}^7F_2$ transition from 610 to 623 nm (figure 8(c)) are electric dipole in nature and are forced by the odd crystal-field Hamiltonian [39, 40]. In addition, and despite the high multiphonon relaxation probability between the ^5D_J ($J = 0$, 1) levels in the emission spectra, one can clearly see in figure 8(b) two peaks from 585 to 589 nm which are associated with the $^5D_1 \rightarrow {}^7F_3$ electric-dipole transition.

The first result that can be extracted from the Eu^{3+} emission spectrum measured at low pressure is the presence of two broad peaks associated with the $^5D_0 \rightarrow {}^7F_0$ transition. This suggests that Eu^{3+} ion occupies two different local distributions of environments, also supported by the

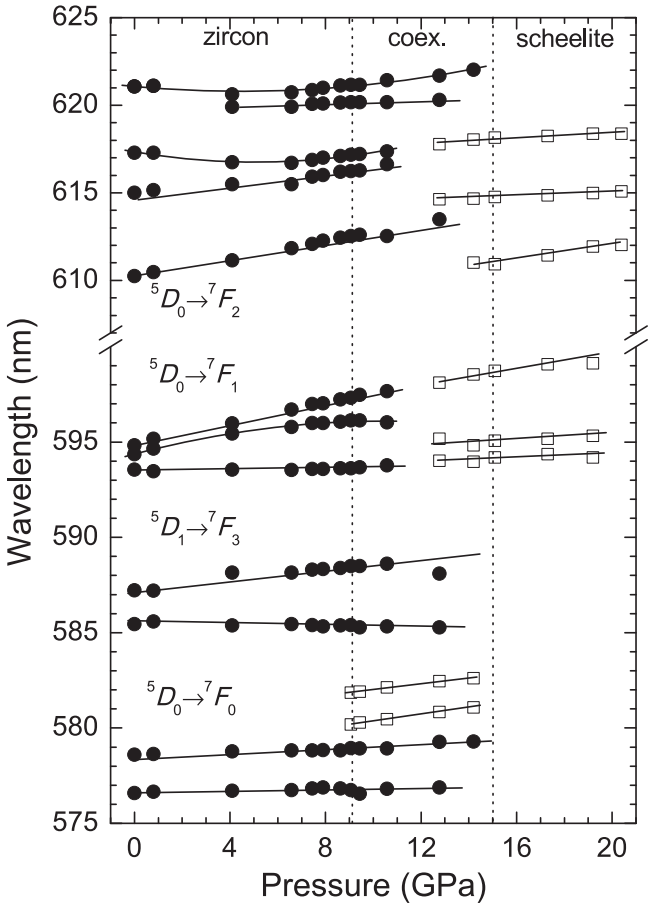

Figure 9. Pressure dependence of the photoluminescence peak positions of YVO_4:Eu^{3+} nanoboxes. The vertical dashed lines show the onset and end of the phase transition. Solid circles and empty squares represent the electronic transitions of the low- and high-pressure phase, respectively. The solid lines are guides for the eye.

inhomogeneous broadening observed in all the emission bands, especially for the $^5D_0 \rightarrow {}^7F_2$ transition. In the zircon-type structure, Y^{3+} only occupies one crystallographic site and Eu^{3+} is expected to replace Y^{3+} ions. However, it has been suggested that in nanoparticles a residual part of Eu^{3+} ions can be located at the surface of the nanoparticles where the number of defects in the crystalline structure can be high. Such environment would give rise to a less intense and broader $^5D_0 \rightarrow {}^7F_0$ peak than in a crystalline environment. This is what we observe in the case of YVO_4:Eu^{3+}, where a comparison between both $^5D_0 \rightarrow {}^7F_0$ peaks suggests that the less intense peak might be due to the residual part of Eu^{3+} ions located near the surface of the nanobox as would be expected by the presence of defects in the YVO_4 nanoparticle [41] and already observed in Y_2O_3:Eu^{3+} nanoparticles [42].

As pressure increases, the photoluminescence spectrum is not largely affected up to 9.1 GPa with the peaks broadening and shifting with pressure (figure 9). Above 9.1 GPa the photoluminescence intensity drops and additional peaks emerge as the consequence of the onset of the phase transition that ends at 15 GPa. As an effect of the amorphization, photoluminescence intensity decreases progressively above 9.1 GPa up to 20.4 GPa when only the three $^5D_0 \rightarrow {}^7F_2$ peaks typical from the scheelite phase can be unequivocally observed [35]. If we concentrate on the analysis of the $^5D_0 \rightarrow {}^7F_0$ peaks (figure 8(a)), which is the most sensitive electronic transition to local environment changes of Eu^{3+}, we can see that the initial gap between the emission peaks of this transition opens slightly with pressure up to 9.1 GPa. In particular, the peak at lower wavelength is pressure independent within our resolution indicating that the defect site is not affected by pressure. When the phase transition has finished (15 GPa) the intensity of both $^5D_0 \rightarrow {}^7F_0$ peaks drops preventing their observation (figure 8 (a)).

Regarding the emission spectra of the $^5D_0 \rightarrow {}^7F_1$ and $^5D_1 \rightarrow {}^7F_3$ Stark peaks (figure 8(b)), from ambient pressure up to 9.1 GPa, the barycenter of the $^5D_0 \rightarrow {}^7F_1$ transition presents a redshift. In contrast, the barycenter of the $^5D_1 \rightarrow {}^7F_3$ transition experiences a blueshift. For the Stark peaks of the $^5D_0 \rightarrow {}^7F_2$ transition, the observation of the phase transition is evident at 12.8 GPa, when three extra peaks at shorter wavelengths (higher energy) emerge. This is the result of a decrease of the effective charge on oxygen atoms in the scheelite phase with respect to the zircon phase, and causes an energy increase of the $^5D_0$ level. Finally, the irreversibility of the phase transition is proven by the spectrum measured at ambient conditions after pressure release, shown at the top of figure 8, in good agreement with XRD and Raman spectroscopy measurements.

4. Conclusions

We have shown with a combined study of XRD, Raman spectroscopy, and Eu^{3+} photoluminescence under high pressure that zircon-type YVO_4:Eu^{3+} nanoboxes undergo an amorphization and a short-range phase transition to scheelite-type structure 2 GPa above the onset previously reported for bulk YVO_4 [15, 16]. The presence of two $^5D_0 \rightarrow {}^7F_0$ Eu^{3+} photoluminescence peaks shows, at least for the low-pressure zircon phase, that Eu^{3+} occupies not only the expected local environment in substitution for Y^{3+}, but also a disordered environment. This new environment is probably present on the surface of the nanoboxes, for which the surface to volume ratio is considerable. Both spectroscopic techniques, Raman spectroscopy and photoluminescence, experience an intensity drop and considerably band broadening of the peaks as a consequence of the amorphization. All the techniques confirm the irreversibility of the amorphization and short-range phase transition to a scheelite-type structure.

Acknowledgments

This work has been performed under financial support from Spanish MINECO under the National Program of Materials (MAT2013-46649-C4-1/2/3/4-P) and the Consolider-Ingenio 2010 Program (MALTA CSD2007-00045). Funding by the Fundación Caja Canarias (ENER-01) and the EU-FEDER funds is also acknowledged. JR-F thanks the Alexander von Humboldt Foundation for a postdoctoral fellowship and NS

thanks the German Research Foundation (DFG) for financial support (Project RA2585/1-1). We acknowledge Diamond Light Source for time on beamline I15 under proposals EE3652 and EE6517. Parts of this research were carried out at the light source PETRA III at DESY (Hamburg), a member of the Helmholtz Association (HFG). We would like to thank H-P Liermann and W Morgenroth for assistance in using beamline P02.2.

References

[1] Piot L, Le Floch S, Cornier T, Daniele S and Machon D 2013 *J. Phys. Chem.* C **117** 11133
[2] Zhang F X, Wang J W, Lang M, Zhang J M, Ewing R C and Boatner L A 2009 *Phys. Rev.* B **80** 184114
[3] Lacomba-Perales R, Errandonea D, Bettinelli M and Meng Y 2010 *Phys. Rev.* B **81** 064113
[4] Yuan H *et al* 2012 *J. Phys. Chem.* C **116** 24837
[5] Mishra A K, Garg N, Pandey K K, Shanavas K V, Tyagi A K and Sharma S M 2010 *Phys. Rev.* B **81** 104109
[6] Wang L *et al* 2010 *Phys. Rev. Lett.* **105** 095701
[7] Mukherjee S, Kim K and Nair S 2007 *J. Am. Chem. Soc.* **129** 6820
[8] Sopu D, Albe K, Ritter Y and Gleiter H 2009 *Appl. Phys. Lett.* **94** 191911
[9] Ozawa L and Itoh M 2003 *Chem. Rev.* **103** 3835
[10] Jüstel T, Nikol H and Ronda C 1998 *Angew. Chem. Int. Ed.* **37** 3084
[11] Zhu Y, Xu W, Zhang H, Wang W, Tong L, Xu S, Sun Z and Song H 2012 *Appl. Phys. Lett.* **100** 081104
[12] Khan A F, Haranath D, Yadav R, Singh S, Chawla S and Dutta V 2008 *Appl. Phys. Lett.* **93** 073103
[13] Cho Y-S and Huh Y-D 2011 *Bull. Korean Chem. Soc.* **32** 335
[14] Jayaraman A, Kourouklis G A, Espinosa G P, Cooper A S and van Uitert L G 1987 *J. Phys. Chem. Solids* **48** 755
[15] Wang X, Loa I, Syassen K, Hanfland M and Ferrand B 2004 *Phys. Rev.* B **70** 064109
[16] Manjón F J, Rodríguez-Hernández P, noz A M, Romero A H, Errandonea D and Syassen K 2010 *Phys. Rev.* B **81** 075202
[17] Ray S, Banerjee A and Pramanik P 2009 *Mater. Sci. Eng.* B **10** 156
[18] Boehler R 2006 *Rev. Sci. Instrum.* **77** 115103
[19] Mao H K, Xu J and Bell P M 1986 *J. Geophys. Res.* **91** 4673
[20] Hammersleya A P, Svensson S O, Hanfland M, Fitch A N and Häusermann D 1996 *High Press. Res.* **14** 235
[21] Holland T J B and Redfern S A T 1997 *Mineral. Mag.* **61** 65
[22] Kraus W and Nolze G 1996 *J. Appl. Crystallogr.* **29** 301
[23] Larson A C and von Dreele R B General structure analysis system *Los Alamos National Laboratory Report LAUR* 86–748
[24] Toby B H 2001 *J. Appl. Crystallogr.* **34** 210
[25] Qiu X, Thompson J W and Billinge S J L 2004 *J. Appl. Crystallogr.* **37** 678
[26] Chupas P J, Qiu X, Hanson J C, Lee P L, Grey C P and Billinge S J L 2003 *J. Appl. Crystallogr.* **36** 1342
[27] Farrow C L, Juhas P, Liu J W, Bryndin D, Božin E S, Bloch J, Proffen T and Billinge S J L 2007 *J. Phys.: Condens. Matter* **19** 335219
[28] Trenque I, Mornet S, Duguet E and Gaudon M 2013 *Inorg. Chem.* **52** 12811
[29] Langford J I and Wilson A J C 1978 *J. Appl. Crystallogr.* **11** 102
[30] Klotz S, Chervin J-C, Munsch P and Marchand G L 2009 *J. Phys. D: Appl. Phys.* **42** 075413
[31] Jeong I-K, Proffen T, Mohiuddin-Jacobs F and Billinge S J L 1999 *J. Phys. Chem.* A **103** 921
[32] Frogley M D, Sly J L and Dunstan D J 1998 *Phys. Rev.* B **58** 12579
[33] Birch F 1978 *J. Geophys. Res.* **83** 1257
[34] Popescu C, Sans J A, Errandonea D, Segura A, Villanueva R and Sapiña F 2014 *Inorg. Chem.* **53** 11598
[35] Chen G, Stump N A, Haire R G, Peterson J R and Abraham M M 1992 *J. Phys. Chem. Solids* **53** 1253
[36] Rivera-López F *et al* 2006 *High Press. Res.* **26** 355
[37] Dieke G H and Crosswhite H M 1963 *Appl. Opt.* **2** 675
[38] Lavín V, Babu P, Jayasankar C K, Martín I R and Rodríguez V D 2001 *J. Chem. Phys.* **115** 10935
[39] Peacock R D 1975 *Struct. Bonding* **22** 83
[40] Oomen E W L J and van Dongen A M A 1989 *J. Non-Cryst. Solids* **111** 205
[41] Song H, Chen B, Peng H and Zhang J 2002 *Appl. Phys. Lett.* **81** 1776
[42] Ray S, León-Luis S F, Manjón F J, Mollar M A, Gomis O, Rodríguez-Mendoza U, Agouram S, Muñoz A and Lavín V 2014 *Curr. Appl. Phys.* **14** 72